J Appl Electrochem (2007) 37:1227–1236
DOI 10.1007/s10800-007-9359-4

ORIGINAL PAPER

A novel method for the preparation of bi-metallic (Pt–Au) nanoparticles on boron doped diamond (BDD) substrate: application to the oxygen reduction reaction

B. El Roustom · G. Siné · G. Fóti · Ch. Comninellis

Received: 14 February 2007 / Revised: 28 June 2007 / Accepted: 28 June 2007 / Published online: 8 September 2007

Abstract A novel method was developed to synthesize bi-metallic nanoparticles (Au–Pt) on boron-doped diamond (BDD) substrate. This method consisted of (a) deposition of a small amount of gold (equivalent to a few monolayers) by sputtering on the BDD surface, (b) heat treatment of the obtained sample at 600 °C in air, resulting in the formation of stable nanoparticles on BDD (Au/BDD electrode), (c) electrodeposition of Pt on the Au/BDD surface occurring preferentially on the Au nanoparticles, and finally (d) heat treatment at 400 °C to enhance the interaction between Au and Pt. The ratio between Au and Pt nanoparticles can be modified by modifying the amount of electrodeposited Pt and was estimated using cyclic voltammetry. These Pt-Au/BDD composite electrodes were used to study oxygen reduction using both potential sweep (cyclic voltammetry) and hydrodynamic (turbine electrochemical cell) methods.

Keywords Au–Pt alloys · Au–Pt nanoparticles · BDD · Electrocatalysis · Oxygen reduction

B. El Roustom · G. Siné · G. Fóti · Ch. Comninellis
Institute of Chemical Sciences and Engineering, Ecole Polytechnique Fédérale de Lausanne (EPFL), Lausanne 1015, Switzerland

B. El Roustom (✉) · Ch. Comninellis (✉)
EPFL-SB-ISIC-GGEC, Station 6, Building CH, Lausanne 1015, Switzerland
e-mail: bahaa.elroustom@epfl.ch

Ch. Comninellis
e-mail: christos.comninellis@epfl.ch

1 Introduction

Interest in the study of nanoparticles has increased during the last decade. It has been reported that metallic nanoparticles exhibit both physical and chemical properties that can be different from those of bulk metal [1]. These observations have motivated much work, covering fields as different as optics, magnetics, electronics and catalysis and electrocatalysis.

Gold is an impressive example of new properties associated with the nanoscale. When highly dispersed on a reducible metal oxide support, gold nanoparticles exhibit surprisingly high activity for CO oxidation even at low temperature [2], whereas bulk gold is usually considered as a weak chemisorber and catalyst. Gold nanoparticles have also shown extraordinary electrocatalytic activity toward the oxygen reduction reaction (ORR) when deposited on a bulk gold electrode substrate [3]. The exploration of effective methods for the preparation of gold and gold-based alloy nanoparticles has led to the development of catalysts of high activity for a variety of oxidation and reduction reactions [4].

Nevertheless, platinum and platinum-based nanoparticle catalysts have been the most widely studied systems, due to their applicability in direct alcohol fuel cell (DAFC) technology [5–8]. Considerable efforts have been made to correlate the activity of such catalysts with their morphology and to reduce the noble metal loading; hence several synthesis methods of nanoscale platinum catalysts have been explored [9–13]. However, during methanol electrooxidation, pure Pt catalysts are readily poisoned by adsorbed intermediates (CO) which block the catalytic sites. Alloying Pt with a second metal yields new catalysts with increased tolerance to CO poisoning thanks to the so-called bifunctional mechanism [14] (in which Pt adsorbs

methanol dissociatively and the second metal activates water at lower potential than Pt does) and/or electronic effects [15] (weakening of the Pt–CO bond).

Regarding the properties of both Au and Pt nanoparticles, recent studies on gold-platinum (Au–Pt) nanoparticle catalysts revealed the viability of preparing alternative electrocatalysts, potentially used for fuel cell reactions such as oxygen reduction and methanol oxidation [16–18]. The catalysis of these two reactions has broad technological applications, including fuel-cell technology at low temperature (<100 °C). The rate of breaking the O–O bond to form water depends strongly on its interaction with the adsorption sites of the catalyst and competition with other species in the electrolyte.

Here we report the use of a new technique to add Pt to Au nanoparticles deposited on BDD electrodes. The advantages of BDD as catalyst support are: (i) it does not form an oxide layer on its surface in aqueous solution, (ii) it shows a high chemical and thermal stability, (iii) it has a very low background current and large electrochemical potential window [19].

The BDD electrode has already been used in our group [20] as a substrate for Au [21], Pt [22–24] and IrO_2 nanoparticles [25, 26] deposited independently, and has also been studied widely in waste water treatment [27–29].

The aim of this work was to develop a new technique enabling preferential deposition of Pt on the Au nanoparticles and the formation of a more homogeneous Au–Pt alloy by heating the composite electrode at 400 °C in air.

2 Experimental

Boron doped diamond (BDD) electrodes were prepared by the hot-filament chemical vapor deposition (HF-CVD) technique on low resistivity (1–3 $\mu\Omega$ cm) p-Si {100} wafers (Siltronix, diameter 10 cm, thickness 0.5 mm). The process gas was a mixture of 1% CH_4 in H_2 containing trimethylboron as doping agent. Film growth occurred at a rate of 0.24 μm h^{-1}. The grain size of the BDD films was between 200 and 800 nm and the film thickness was about 1 μm. The boron/carbon atomic ratio in the BDD film was 2500 ppm; this corresponds to a carrier concentration of 4.9×10^{20} atom cm^{-3}. Before use, the as-grown boron-doped diamond electrodes were washed once with 2-propanol and twice with Milli-Q water in an ultrasonic bath.

Gold was deposited onto the BDD substrate by a sputtering technique in an inert atmosphere at room temperature, using conditions: direct current (dc) mode with a discharge of 330 V, and an argon pressure of 10^{-2} mbar. Under these conditions, the deposition rate was 0.09 nm s^{-1} on a smooth surface, as determined by profilometric measurement (Alphastep, Model 500) of the film thickness (in the 5–30 nm range) on smooth silicon samples processed simultaneously. This is in very good agreement with the mass deposition rate of 0.17 μg s^{-1} per 1 cm^2 geometrical surface area obtained by atomic adsorption spectroscopic analysis (Shimadzu, Model AA-6650) after complete dissolution of the gold deposit in *aqua regia* at 80 °C in 30 min. The gold deposits prepared by short-time (20 s) sputtering were then heated at 600 °C in air to obtain stable gold nanoparticles with an average diameter of approximately 15 nm.

Electrochemical deposition of Pt on the Au/BDD composite electrode was carried out under potentiostatic conditions, from deaerated 1 M $HClO_4$ solution containing 2 mM H_2PtCl_6, by applying a potential step from 1 to 0.02 V vs. SHE for a given time.

Electrochemical measurements were performed in a conventional three-electrode cell using a computer-controlled potentiostat (Autolab PGstat30). The BDD thin film electrodes, modified by Au or Au–Pt deposits were used as working electrodes (0.8 cm^2 exposed area), $Hg/Hg_2SO_4 \cdot K_2SO_4$(sat) as reference electrode and a platinum wire as counter electrode. 0.5 M H_2SO_4 solution was made with ultra-pure water (Milli-Q). This solution was saturated with oxygen after bubbling oxygen during 45 min. All potentials in this work are reported with respect to the standard hydrogen electrode (SHE).

The composite electrodes were used to study the ORR using potential sweep (cyclic voltammetry) and hydrodynamic methods. Rotating disk electrode (RDE) has been widely used in hydrodynamic methods; however, the main limitation of this system is the manufacture of RDE based on BDD electrodes. This has motivated us in the development of a new system (turbine electrochemical cell) in order to use BDD plates in hydrodynamic systems.

The turbine electrochemical cell operates with a rotating electrolyte. In ontrast to the classical rotating electrode, the working electrode (BDD) is fixed and the solution is agitated by a turbine (Fig. 1a). The turbine cell comprised a copper conductor on which the diamond electrode was laid. The contact was provided by a silver paste (EPO-TEK 410E, Polyscience AG, Cham, CH). The geometric area was 0.8 cm^2 and the cell volume 50 cm^3.

The hydrodynamic theory for the turbine cell was developed recently in our group [30]. The limiting current and the diffusion boundary thickness obtained after resolution of the convective-diffusion equation are the following:

$$j_{\lim} = 0.62nFAD_j^{2/3}\omega^{1/2}v^{-1/6}C_j^* \quad (1)$$

$$\delta = 1.61D_j^{1/3}\omega^{-1/2}v^{1/6} \quad (2)$$

where $j_{\lim}$ is the limiting current, F the Faraday constant, A the geometrical area of the electrode, C^* the concentration

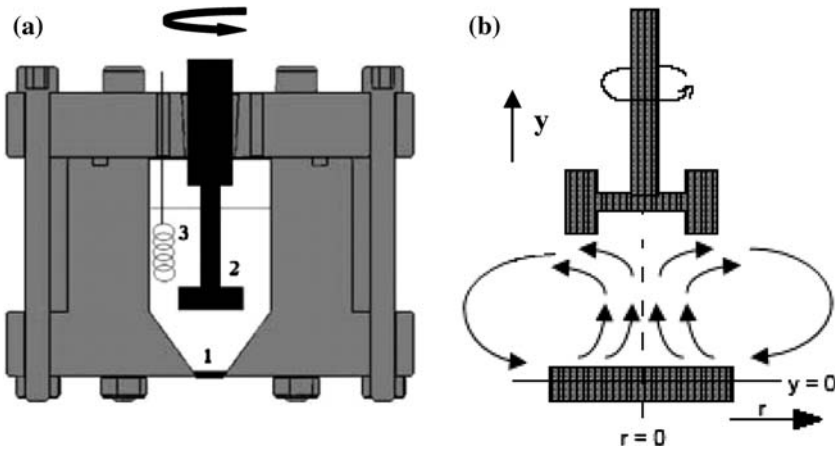

Fig. 1 (**a**) Schematic presentation of the turbine cell, (1) WE, (2) turbine, (3) CE; (**b**) Schematic presentation of electrolyte flow

of species in the bulk, D the diffusion coefficient, ω the angular velocity of the stirrer, v the kinematic viscosity of the solution and δ the thickness of the diffusion layer.

The surface morphology of the samples was characterized by scanning electron microscopy (SEM) using a JEOL JMS-6300-F scanning electron microscope at a magnification of up to 60000 times. Identification of oxidation states of metals in the different samples was performed by X-ray Photoelectron Spectroscopy (XPS) carried out with a Kratos Axis-Ultra spectrometer using a monochromatic Al K_α X-ray source, operated at 15 kV and pass energy of 20 eV. A total area of 700 × 300 μm was investigated over a thickness of 50–100 Å. Peaks of interest in the signals (Pt*4f* and Au*4f*) were deconvoluted using CasaXPS® computer software (Casa Software Ltd).

3 Results and discussion

The bimetallic Pt–Au/BDD electrode was prepared after electrodeposition of Pt on the Au/BDD composite electrode developed previously [21].

3.1 Deposition of Au on BDD

A very low loading of gold (equivalent to a few monolayer average thickness in a continuous film) was deposited on the BDD electrode using the sputtering technique. Gold deposits in the as-sputtered state, *i.e.* without any subsequent heat treatment, have been characterized as a function of the deposited amount of gold. Sputtering was performed onto non-treated (rough) BDD surface at ambient temperature under identical operation conditions excepting the time of exposition, varied in the range of 5–40 s. The constant deposition rate was 0.09 nm s^{-1} referring to a smooth surface. This corresponds to a rate of 5.3×10^{14} atom s^{-1} on 1 cm^2 geometrical surface area, which would be equivalent to about 0.35 monolayers of gold per second. In the case of short-time (≤40 s) sputtered deposits, which were of special interest for subsequent stabilization of nanoparticles by heat treatment, the small amount of deposited gold and its very high dispersion did not allow the characterization of the samples by SEM. The method of choice for the characterization of as-sputtered deposits was cyclic voltammetry in a supporting electrolyte containing no electroactive solute.

Cyclic voltammetric analysis was made in 0.5 M H_2SO_4 at 25 °C, between inversion potentials of 0.64 and 1.80 V with a scan rate of 100 mV s^{-1}. As-sputtered gold deposits were not stable even under such conditions of cyclic voltammetric analysis, i.e., in the absence of any electroactive species, as illustrated in a previous paper [21] by the evolution of the voltammogram during continuous potential cycling. The particles of gold were highly unstable and inappropriate for electrochemical applications.

For the stabilization of the highly dispersed unstable populations of as-sputtered gold particles, a heat treatment procedure has been proposed. The nanosize deposits obtained were characterized by electrochemical methods and by scanning electron microscopy (SEM). The properties of the deposits depended on several parameters; two of them have been studied in detail: (*i*) the temperature of the post-deposition heat treatment, and (*ii*) the amount of sputter-deposited gold [21]. Particles with an average diameter between 15 and 40 nm depending on the amount of deposited gold were formed (Fig. 2). These particles were stable and suitable for electrochemical and electrocatalytic applications.

3.2 Electrodeposition of Pt on Au/BDD

The electrodeposition of platinum was performed on the Au/BDD electrode under potentiostatic conditions. The amount of deposited Pt can be controlled using the electrodeposition time. It was estimated by integrating the charge density of the *j–t* curve. Conditions for Pt electrodeposition on

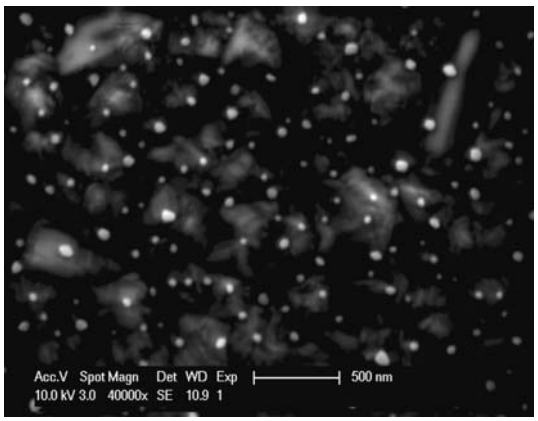

Fig. 2 SEM photomicrograph of a gold deposit (1.1×10^{16} gold atoms per 1 cm^2 geometrical surface area) on polycrystalline BDD substrate heated to 600 °C

Au/BDD electrodes were the following: a potential step from 1 to 0.02 V vs. SHE was applied for 5 s to a deaerated 1 M $HClO_4$ + 2 mM H_2PtCl_6 solution. A typical current-time transient for the electrodeposition of Pt on Au/BDD composite electrode is shown in Fig. 3

During electrodeposition the current initially increased due to the growth of independent nuclei or formation of new nucleation sites without overlapping effects. This current increased to a maximum value j_m at a time t_m corresponding to overlapping between the nuclei. Finally, the current decreased due to overlapping of diffusion zones of different nuclei and coalescence of growing centers. From time t_m corresponding to j_m the current decreased due to the decrease in the surface area of deposited platinum particles, and it can then be considered that a change from hemispherical to linear mass transfer diffusion occurred because of particle size increase.

In the domain of free growth of nuclei, the *j–t* curve can be plotted in order to yield linear j^2 vs. *t* plots. This indicates a 3D-nucleation process on hemispherical nuclei with diffusion control [31]. On the basis of this behavior, Scharifker and Hills [32] have developed a theoretical model that allows the determination of the nucleation mode between the instantaneous or progressive mechanisms. In the instantaneous nucleation mechanism, all the nuclei are rapidly created during the first stages of the process and their number remains constant throughout. In the progressive nucleation mechanism, new nuclei are continuously formed during the whole deposition process, because the nucleation rate is low. At the same time, the primary nuclei growth takes place. Figure 4 shows the experimental *j–t* curve plotted in reduced variables (curve a), as well as those relative to the two mechanisms (curve b and curve c for progressive and nucleation mechanisms, respectively). It can be seen on Fig. 4 that the experimental curve fits between the two mechanisms, in better agreement with that for a progressive nucleation. Therefore it can be concluded that Au nanoparticles, pre-modifying the diamond surface, act like preferential nucleation sites.

3.3 Morphological characterization

The Pt–Au/BDD composite electrode was investigated using scanning electron microscopy (SEM). Typical SEM micrographs of the composite electrode after Pt electrodeposition are shown in Fig. 5. This shows (in comparison with Fig. 2) that the average diameter of the particles increased after Pt deposition. However, the dispersion of the particles did not change, indicating that Pt particles are deposited preferentially on Au particles.

X-ray photoelectron spectroscopy (XPS) was also conducted on Pt–Au/BDD composite electrodes before and after heat treatment. Figure 6a shows the XPS survey spectrum of such an electrode. Contributions from both metals (Au*4f* doublet at 80–90 eV and Pt*4f* doublet at

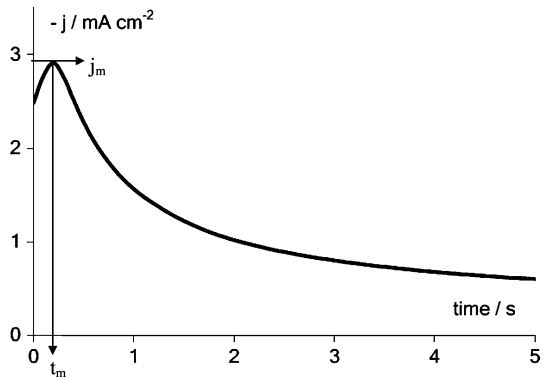

Fig. 3 Chronoamperogram of the electrodeposition of Pt on a Au/BDD composite electrode. Potential step from +1 to +0.02 V vs SHE, during 5 s in 2 mM H_2PtCl_6 + 1 M $HClO_4$ solution at 25 °C. j_m is the maximum current density and t_m is the corresponding time

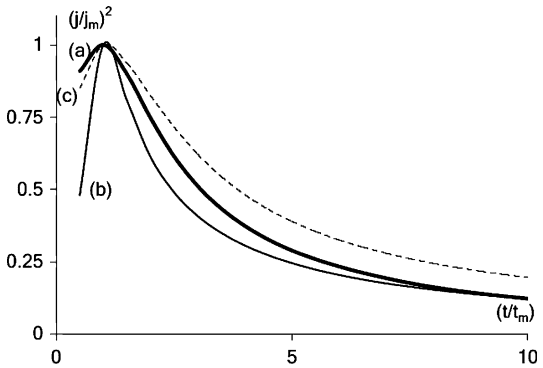

Fig. 4 Response of Pt electrodeposition on Au/BDD electrode plotted in reduced variables. (**a**) Experimental values. (**b**) theoretical data for progressive nucleation [31]. (**c**) theoretical data for instantaneous nucleation [31]

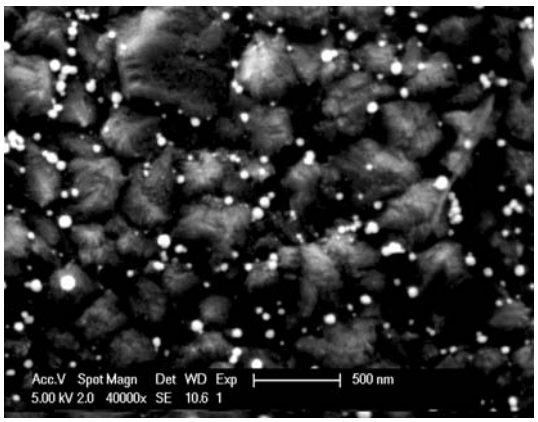

Fig. 5 SEM photomicrograph of a gold deposit (1.1×10^{16} gold atoms per 1 cm^2 geometrical surface area) on polycrystalline BDD substrate heated to 600 °C after Pt electrodeposition (3×10^{16} platinum atoms per 1 cm^2 geometrical surface area)

70–80 eV) are evident from Fig. 6a, confirming the presence of both Au and Pt on the diamond surface. However, this analysis gives only poor insight into the structure of the deposit, as the whole depth of particles is analysed by XPS. Finally, the two peaks attributed to the contribution of C*1s* (280–290 eV) and O*1s* (530–540 eV) are due to the underlying diamond substrate and interactions with atmospheric oxygen, respectively.

The CasaXPS® software was used to perform the deconvolution of the Pt*4f* and Au*4f* signals in order to determine the respective oxidation states of these two metals. Deconvoluted XPS doublets of Pt*4f* and Au*4f* in Pt-Au/BDD composite electrodes are shown in Fig. 6b and c, respectively. The Pt*4f* signal was composed of four main contributions (peaks 1–4 on Fig. 6b). Peaks 1 and 2 can be attributed to $Pt4f_{7/2}$ and $Pt4f_{5/2}$ lines of metallic Pt, respectively, whereas peaks 3 and 4 can be attributed to $Pt4f_{7/2}$ and $Pt4f_{5/2}$ lines of Pt(II) present, for instance in PtO or $Pt(OH)_2$. The ratio between metallic and oxidized forms of Pt was about 3:1. In contrast, the Au*4f* doublet was composed only of two well-defined Gaussian peaks (peaks 1 and 2 on Fig. 6c). The peaks can be attributed to $Au4f_{7/2}$ and $Au4f_{5/2}$ of metallic Au, respectively, and there was no other contribution.

3.4 Electrochemical characterization

Figure 7 shows cyclic voltammograms recorded in N_2-saturated 0.5 M H_2SO_4 solution at (a) a Au/BDD composite electrode, (b) a 40Pt–60Au/BDD (nominal composition) composite electrode before heat treatment and (c) after heat treatment in air at 400 °C. In the forward scan, the onset potential for the formation of gold oxide (AuO_x) is 1.3 V. In the reverse scan, the reduction of AuO_x occurred at a potential of 1.08 V. After Pt electrodeposition the peak of

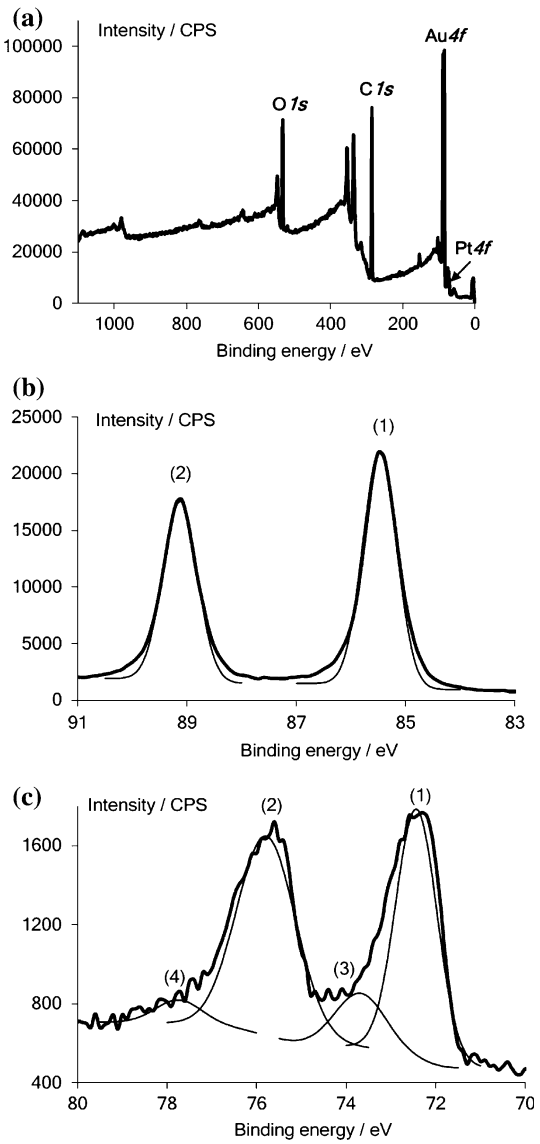

Fig. 6 (**a**) XPS survey spectrum of the 20Pt–80Au/BDD electrode (nominal composition); (**b**) XPS deconvoluted Au*4f* doublet and (**c**) Pt*4f* doublet of a 20Pt-80Au/BDD (nominal composition) electrode

AuO_x reduction disappeared. This was a clear indication that Pt has been deposited on Au nanoparticles and covered them. After heat treatment at 400 °C in air the peak of AuO_x reduction reappeared at the surface with a smaller intensity, but at the same potential. The heat treatment helped the Au nanoparticles to reappear at the surface of the composite electrode and led to the formation of bimetallic nanoparticle surfaces.

The cyclic voltammogram of the Pt–Au/BDD electrode before heat treatment was very similar to that obtained with pure Pt. We can clearly distinguish the formation of platinum oxide (PtO_x), starting at about 0.85 V up to oxygen evolution shifted from 1.7 (Au/BDD) to 1.5 V. The peak of PtO_x reduction appeared clearly at 0.58 V. After heat

treatment in air at 400 °C, the forward scan shows that the formation of PtO_x and AuO_x starting at about 0.95 V, was then masked by the oxygen evolution starting at 1.63 V (between the potential of oxygen evolution at Au/BDD and untreated Pt–Au/BDD composite electrodes). In the reverse scan, the peak of PtO_x reduction decreased and shifted to lower potentials (0.47 V), showing a more difficult reduction of PtO_x. These results indicate that the interaction between Au and Pt in the nanoparticles was reinforced due to the heat treatment of the Pt–Au/BDD composite electrode.

The results of the cyclic voltammetric experiment, contrary to the results from SEM and XPS, proved that significant modification occurred at the surface of the Pt–Au/BDD composite electrode during heat treatment. By integrating the cathodic charges of the peaks of AuO_x reduction (482 μC cm^{-2} for one monolayer) and PtO_x reduction (496 μC cm^{-2} for one monolayer), the real composition of the catalytic surface of the composite electrode in contact with the electrolyte can be estimated. This mass composition of the surface is different from the bulk, nominal composition. Table 1 shows experimental values calculated from the cyclic voltammograms in Fig. 7. It gathers the peak potential of AuO_x and PtO_x reduction (E_p), the cathodic charge (Q_p), the ratio between the cathodic charge and the cathodic charge relative to one monolayer (Q_p/Q_m), the potential of oxygen evolution (E_O) and the surface composition.

3.4.1 *Effect of heat treatment*

The effect of the temperature of heat treatment was studied to investigate the behavior of the Pt–Au/BDD composite electrode. Figure 8 shows typical voltammograms for (a) the Au/BDD electrode, (b) the 80Pt–20Au/BDD (nominal composition) composite electrode before heat treatment and (c) after heat treatment in air at 200 °C and (d) at 400 °C. After Pt electrodeposition the peak of AuO_x reduction disappeared. The peak of PtO_x reduction appeared and the overpotential for oxygen evolution decreased. After heat treatment at 200 °C, the peak of PtO_x reduction decreased slightly and the overpotential for oxygen evolution increased slightly. The peak of AuO_x reduction appeared only after heat treatment at 400 °C. The peak of PtO_x reduction shifted to lower potentials and the overpotential for oxygen evolution increased. The experimental data given in Table 2 imply that when the temperature of heat treatment increases from 200 to 400 °C, the abundance of Au at the surface increases from 5 to 15%.

3.4.2 *Effect of the amount of electrodeposited Pt*

Three different samples of Pt–Au/BDD composite electrode were prepared keeping the amount of Au constant and increasing the amount of electrodeposited Pt, by increasing the time of electrodeposition from 3 to 12 s. The nominal mass compositions were 20Pt–80Au, 40Pt–60Au and 80Pt–20Au.

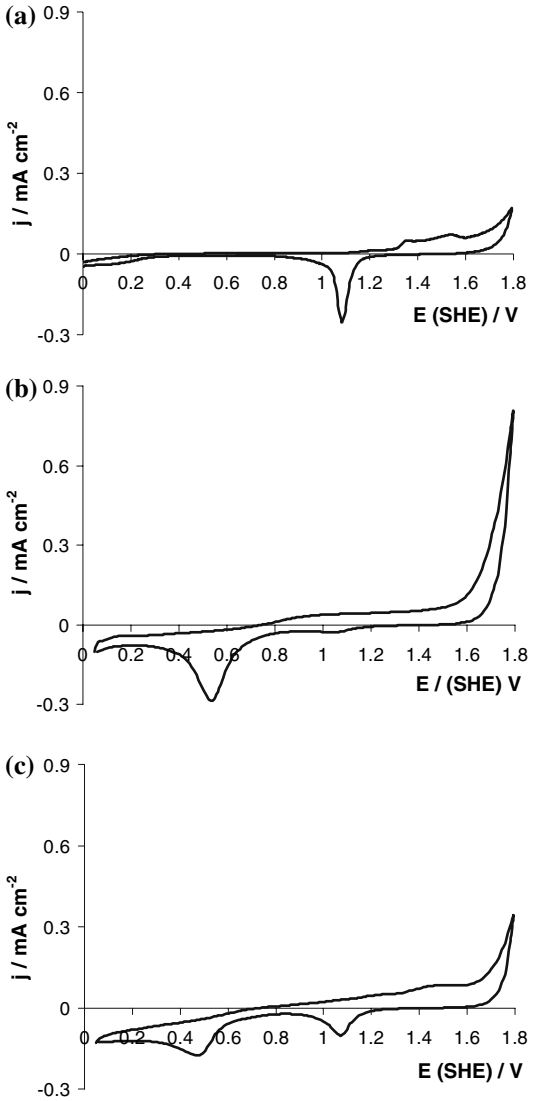

Fig. 7 Cyclic voltammograms of (**a**) Au/BDD electrode, (**b**) 40Pt–60Au/BDD (nominal composition) composite electrode before heat treatment and (**c**) after heat treatment in air at 400 °C. Recorded in N_2 saturated 0.5 M H_2SO_4 solution. V = 50 mV s^{-1}. Geometrical surface = 0.8 cm^2, T = 25 °C

Figure 9a shows the response of the 20Pt–80Au/BDD (nominal composition) electrode before and after heat treatment at 400 °C. The current peak due to AuO_x reduction at 1.08 V disappeared even when a small amount of Pt was deposited. After heat treatment, the Au reappeared at the surface and the peak of PtO_x reduction decreased slightly and shifted to lower potentials. The surface composition of this sample, estimated from the CV measurements, was 45Pt–55Au.

Table 1 Experimental values calculated from the cyclic voltammograms in Fig.7

Electrode	Au			Pt			E_O	Estimated surface composition
	E_p(SHE)/V	Q_p/mC cm^{-2}	Q_p/Q_m	E_p(SHE)/V	Q_p/mC cm^{-2}	Q_p/Q_m		
Au/BDD	1.08	0.40	0.83	–	–	–	1.79	100Au
40Pt–60Au/BDD	–	–	–	0.52	1.25	2.52	1.64	99Pt–1Au
40Pt–60Au/BDD heated	1.06	0.19	0.39	0.45	0.6	1.21	1.72	75Pt–25Au

E_p is the peak potential of AuO_x and PtO_x reduction, Q_p is the cathodic charge, Q_p/Q_m is the ratio between the cathodic charge and that relative to one monolayer, E_O is the potential of oxygen evolution

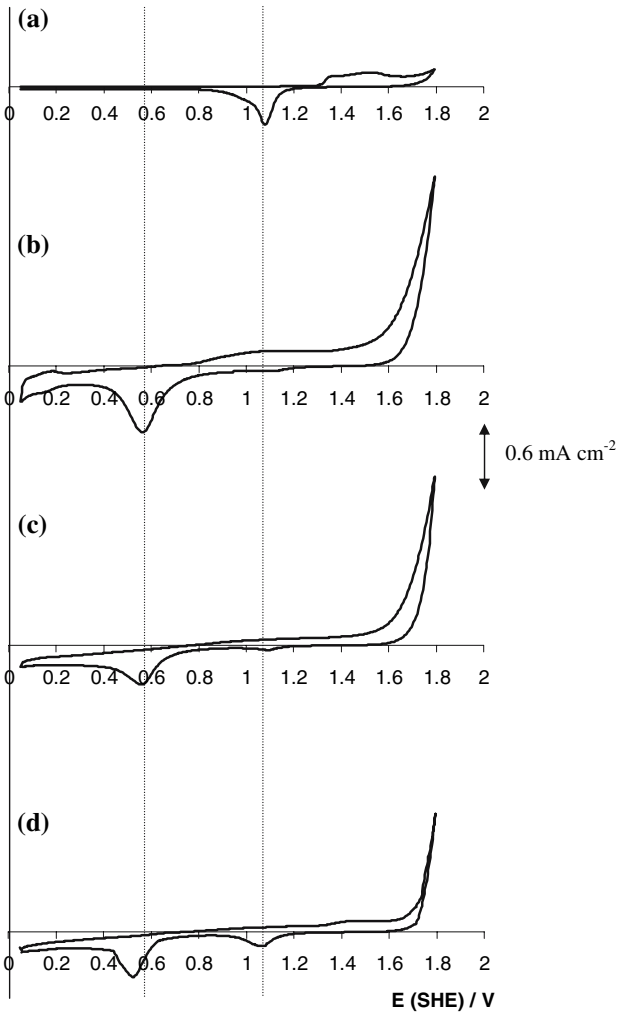

Fig. 8 Cyclic voltammograms of (a) Au/BDD electrode, (b) 80Pt-20Au/BDD (nominal composition) composite electrode before heat treatment, (c) after heat treatment in air at 200 °C and (d) at 400 °C. Recorded in N_2 saturated 0.5 M H_2SO_4 solution. V = 50 mV s^{-1}. Geometrical surface = 0.8 cm^2, T = 25 °C

Figure 9b and c show that when the amount of electrodeposited Pt was increased the ratio of Au at the electrode surface after heat treatment decreased significantly. The estimated surface composition was 75Pt–25Au and 85Pt–15Au for the electrodes with nominal composition of 40Pt–60Au (nominal composition) and 80Pt–20Au (nominal composition), respectively.

3.5 Oxygen reduction reaction

The oxygen reduction reaction was studied on BDD, Au/BDD and Pt–Au/BDD electrodes, in oxygen saturated 0.5 M H_2SO_4 solution, using cyclic voltammetry and a turbine electrochemical cell (equivalent to a rotating disc electrode).

Figure 10 shows cyclic voltammograms of oxygen reduction carried out on BDD, Au/BDD, and 80Pt–20Au/BDD (nominal composition) before and after heat treatment at 400 °C in air. The overpotential for oxygen reduction decreased due to modification of diamond by metallic nanoparticles. The magnitude of the reduction current peak did not change significantly after modification of BDD by Au nanoparticles (Au/BDD). In contrast, that current increased by a factor of two after Pt deposition (sample with a nominal composition of 80Pt–20Au both before and after heat treatment). Table 3 summarizes characteristic data of the experiments shown in Fig. 10.

The kinetics of the oxygen reduction reaction with the composite electrodes were also studied using the turbine electrochemical cell. Figure 11 shows the j–E curves obtained in the turbine cell with Au/BDD, 20Pt–80Au/BDD (nominal composition) and 80Pt–20Au/BDD (nominal composition). In the case of the Au/BDD electrode the limiting current was not well defined. When Pt was added, the limiting current became well defined and its value increased by a factor of two, as found using cyclic voltammetry, when Pt was deposited on the Au/BDD electrode. Also, the overpotential for oxygen reduction decreased after Pt electrodeposition, the potential being at approximately 0.4 V for the Au/BDD electrode and at approximately 0.8 V for the 80Pt–20Au/BDD (nominal composition) electrode.

Figure 12 shows the linear relationship between the current intensity and the square root of the rotation rate of the turbine, in agreement with the Levich equation. The gradients of the lines were calculated using Eq. 1, the ratio between the different slopes being dictated by the ratios of

Table 2 Experimental values calculated from the cyclic voltammograms in Fig. 8

Electrode	Au			Pt			E_O	Estimated surface composition
	E_p(SHE)/V	Q_p/mC cm^{-2}	Q_p/Q_m	E_p(SHE)/V	Q_p/mC cm^{-2}	Q_p/Q_m		
Au/BDD	1.07	0.5	1.04	–	–	–	1.79	100Au
80Pt–20Au/BDD	–	–	–	0.55	2.4	4.8	1.58	99Pt–1Au
80Pt–20Au/BDD (200°C)	1.07	0.05	0.1	0.55	1	2.5	1.64	95Pt–5Au
80Pt–20Au/BDD (400°C)	1.04	0.12	0.25	0.48	0.7	1.4	1.71	85Pt–15Au

E_p is the peak potential of AuO_x and PtO_x reduction, Q_p is the cathodic charge, Q_p/Q_m is the ratio between the cathodic charge and that relative to one monolayer, E_O is the potential of oxygen evolution

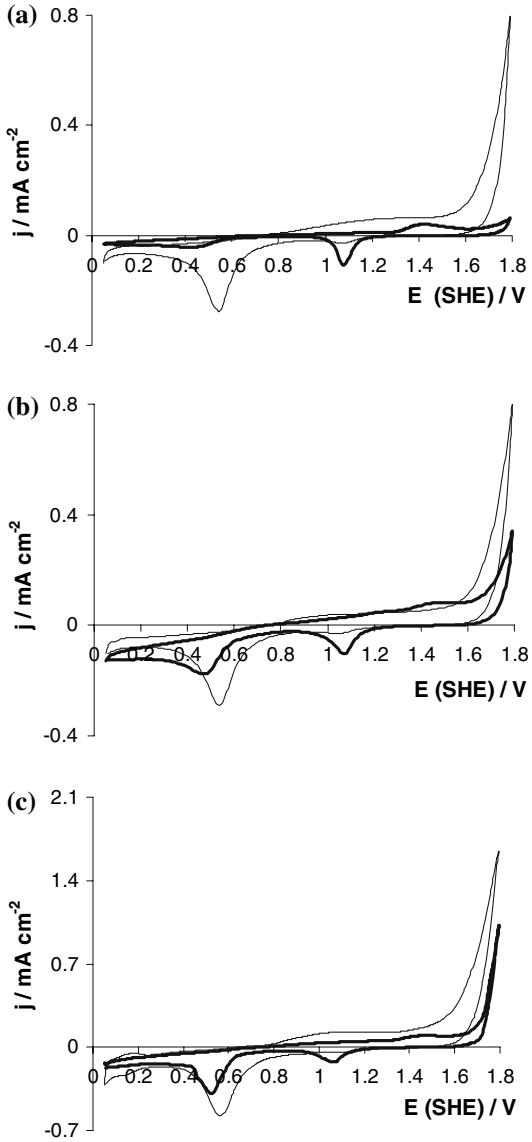

Fig. 9 Cyclic voltammograms of (a) 20Pt–80Au/BDD (nominal composition), (b) 40Pt-60Au/BDD (nominal composition) and (c) 80Pt–20Au/BDD (nominal composition) composite electrodes before heat treatment (thin line), after heat treatment in air at 400 °C (thick line). Recorded in N_2 saturated 0.5 M H_2SO_4 solution. V = 50 mV s^{-1}. Geometrical surface = 0.8 cm^2, T = 25 °C

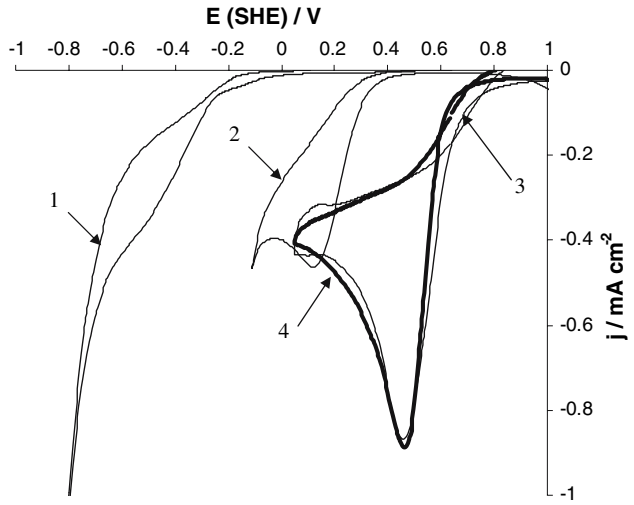

Fig. 10 Cyclic voltammograms of the oxygen reduction reaction for (1) BDD, (2) Au/BDD, (3) 80Pt-20Au/BDD (nominal composition) composite electrode before heat treatment (estimated surface composition 99Pt-1Au/BDD), and (4) after heat treatment in air at 400 °C (estimated surface composition 85Pt–20Au/BDD) in oxygen saturated 0.5 M H_2SO_4 solution. V = 50 mV s^{-1}, geometrical surface = 0.8 cm^2, T = 25 °C

the apparent electron stoichiometries. It was found that the electron stoichiometry increased by a factor of two after Pt deposition, implying a change in the oxygen reduction mechanism. Therefore, we can speculate that O_2 was reduced via a 2 electron mechanism to H_2O_2 on Au/BDD and via a 4 electron mechanism to H_2O on the Pt-Au/BDD composite electrode.

4 Conclusion

A novel method was developed for the preparation of bi-metallic Pt–Au nanoparticles deposited on BDD substrates (Pt–Au/BDD). This method consists of four consecutive steps: (a) deposition of a small amount of gold (equivalent to few monolayers) by sputtering, (b) heat treatment at 600 °C in air, (c) electrodeposition of Pt on the

Table 3 Experimental values calculated from the cyclic voltammograms in Fig. 10

Nominal composition	Estimated surface composition	E vs SHE at 0.02 mA/V	E_{peak} vs SHE/V	j_{peak} /mA cm^{-2}
BDD	–	–0.25	–0.51	0.37
Au/BDD	100Au	0.40	0.11	0.46
80Pt–20Au/BDD	99Pt–1Au	0.78	0.45	0.88
80Pt–20Au/BDD treated	85Pt–15Au	0.78	0.45	0.88

E, (I = 0.02 mA) is the potential of the beginning of the reaction, E_{peak} is the peak potential and j_{peak} is the peak current density

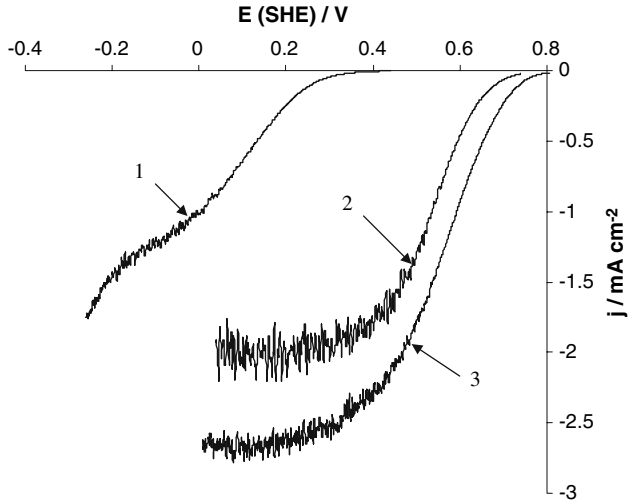

Fig. 11 j–E curves obtained with turbine electrochemical cell for (1) Au/BDD, (2) 20Pt–80Au/BDD (nominal composition) composite electrode and (3) 80Pt–20Au/BDD (nominal composition) composite electrode in oxygen saturated 0.5 M H_2SO_4 solution. Rotation rate: 400 rpm. Geometrical surface = 0.8 cm^2, T = 25 °C

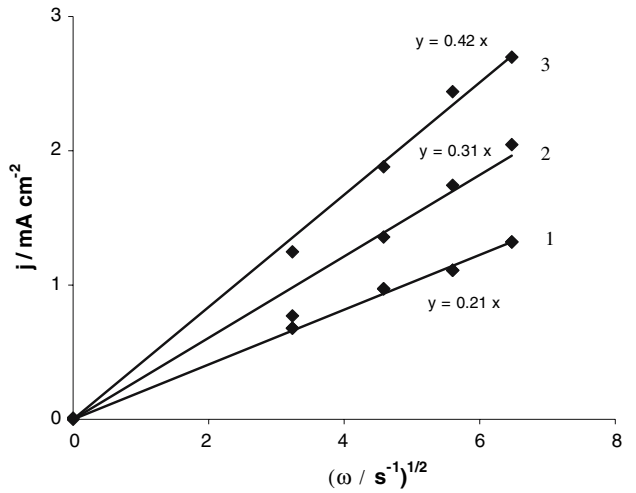

Fig. 12 Levich plot of the data in Fig. 11 from turbine electrochemical cell experiments. (1) Au/BDD, (2) 20Pt–80Au/BDD (nominal composition) and (3) 80Pt–20Au/BDD (nominal composition)

Au/BDD surface, (d) heat treatment at 400 °C in air. It has been shown that Pt was electrodeposited preferentially on the Au nanoparticles. Even if a small amount of Pt was deposited, it covered the entire Au surface and the current peak of AuO_x reduction disappeared from the cyclic voltammogram. After heat treatment of the Pt–Au/BDD sample, Au reappeared at the surface of the nanoparticles and the peak of PtO_x reduction decreased and shifted to lower potential, implying an intimate interaction between Au and Pt. The kinetics of oxygen reduction were enhanced by electrodeposition of Pt on Au/BDD, cyclic voltammetry and measurements with a turbine cell indicating an increase in electron stoichiometry from two to four, corresponding to H_2O_2 being further reduced to water on Pt–Au nanoparticles.

Acknowledgements Financial support from the *Fonds National Suisse de la Recherche Scientifique* is gratefully acknowledged. The authors are thankful to the Swiss Center for Electronics and Microtechnology (CSEM, Neuchâtel) for providing BDD electrodes and to the Thin Film Physics Laboratory (LPCM) and the Interdisciplinary Center of Electron Microscopy (CIME), both at the *Ecole Polytechnique Fédérale de Lausanne* (EPFL), for gold sputtering and SEM analysis, respectively.

References

1. Nakanishi M, Takatani H, Kobayashi Y, Hori F, Taniguchi R, Iwase A, Oshima R (2005) Appl Surf Sci 241:209
2. Haruta M, Ueda A, Tsubota S, Torres Sanchez RM (1996) Catal Today 29:443
3. El-Deab MS, Ohsaka T (2002) Electrochem Com 4:288
4. Haruta M (1997) Catal Today 36:153
5. Aricò AS, Srinivasan S, Antonucci V (2001) Fuel Cells 1:133
6. Lamy C, Lima A, LeRhun V, Delime F, Coutanceau C, Leger J-M (2002) J Power Sources 105:283
7. Parsons R, VanderNoot T (1988) J. Electroanal Chem 257:9
8. Wasmus S, Kuver A (1999) J. Electroanal Chem 461:14
9. Gloaguen F, Leger JM, Lamy C, Marmann A, Stimming U, Vogel R (1999) Electrochim Acta 44:1805
10. Lee S-A, Park K-W, Choi J-H, Kwon B-K, Sung Y-E (2002) J Electrochem Soc 149:A1299
11. Niu Y, Crooks RM (2003) Comptes Rendus Chimie 6:1049
12. Shen P, Chi N, Chan K-Y, Phillips DL (2001) Appl Surf Sci 172:159
13. Solla-Gullon J, Montiel V, Aldaz A, Clavilier J (2000) J Electroanal Chem 491:69
14. Watanabe M, Motoo S (1975) J Electroanal Chem 60:267
15. Park K-W, Choi J-H, Kwon B-K, Lee S-A, Sung Y-E, Ha H-Y, Hong S-A, Kim H, Wieckowski A (2002) J Phys Chem B 106:1869
16. Luo J, Lou Y, Maye MM, Zhong C-J, Hepel M (2001) Electrochem Com 3:172

17. Luo J, Maye MM, Lou Y, Han L, Hepel M, Zhong CJ (2002) Catal Today 77:127
18. Zhong CJ, Maye MM (2001) Adv Mat 13:1507
19. Pleskov YV (1999) Russ Chem Rev 68:381
20. Siné G, Duo I, El Roustom B, Fóti G, Comninellis Ch (2006) J Appl Electrochem V36:847
21. El Roustom B, Foti G, Comninellis Ch (2005) Electrochem Com 7:398
22. Montilla F, Morallon E, Duo I, Comninellis Ch, Vazquez JL (2003) Electrochim Acta 48:3891
23. Siné G, Comninellis Ch (2005) Electrochim Acta 50:2249
24. Siné G, Foti G, Comninellis Ch (2006) J Electroanal Chem 595:115
25. Duo I (2003) Thesis No 2732: EPFL-1015 Lausanne, Switzerland
26. El Roustom B (2006) Thesis No 3624: EPFL-1015 Lausanne, Switzerland
27. Fóti G, Gandini D, Comninellis C, Perret A, Haenni W (1999) Electrochem Solid-State Lett 2:228
28. Gandini D, Mahé E, Michaud PA, Haenni W, Perret A, Comninellis Ch (2000) J Appl Electrochem V30:1345
29. Iniesta J, Michaud PA, Panizza M, Cerisola G, Aldaz A, Comninellis Ch (2001) Electrochim Acta 46:3573
30. Marselli B (2004) Thesis No 3057: EPFL-1015 Lausanne, Switzerland
31. Paunovic M, Schlesinger M (1998) Fundamentals of electrochemical deposition. New York: John Wiley & Sons, Inc
32. Scharifker B, Hills G (1983) ElectrochimActa 28:879